Journal of Alloys and Compounds 780 (2019) 574–580

Contents lists available at ScienceDirect

Journal of Alloys and Compounds

journal homepage: http://www.elsevier.com/locate/jalcom

Enhancing the coercivity of Nd-Fe-B sintered magnets by consecutive heat treatment–induced formation of Tb-diffused microstructures

Sumin Kim [a, 1], Dong-Su Ko [b, 1], Hyun-Sook Lee [a], Donghwan Kim [c], Jong Wook Roh [d, **], Wooyoung Lee [a, *]

[a] Department of Materials Science and Engineering, Yonsei University, Seoul 03722, Republic of Korea
[b] Platform Technology Lab, Samsung Advanced Institute of Technology, Samsung Electronics, Gyeonggi-do 16678, Republic of Korea
[c] R&D Center, Star Group, Daegu 42714, Republic of Korea
[d] School of Nano & Materials Science and Engineering, Kyungpook National University, Gyeongsangbuk-do 37224, Republic of Korea

ARTICLE INFO

Article history:
Received 23 August 2018
Received in revised form
30 October 2018
Accepted 30 November 2018
Available online 3 December 2018

Keywords:
Magnetism
Grain-boundary diffusion
Rare earth
Magnetic properties
Core-shell microstructure

ABSTRACT

Herein, we probed the microstructure of Tb-diffused Nd-Fe-B magnets to investigate the relationship between Tb-diffused area and coercivity enhancement, employing prolonged stepwise heat treatment to ensure sufficient diffusion of Tb in relatively large-size magnets and revealing that this stepwise annealing generated core-shell structures. Quantitative compositional changes pertaining to individual phases of the multiphase system in each heat treatment process were analyzed by constructing ternary diagrams based on electron probe microanalysis compositional maps. During the grain boundary diffusion process, coercivity increased from 15.28 to 24.86 kOe, while only negligible remanence and energy product decreases were concomitantly observed. Microstructure analysis suggested that coercivity was closely related to the concentration and distribution of Tb; more precisely, the above-mentioned core-shell structures successfully suppressed the nucleation of reverse domains at Nd-rich phase/main phase interfaces and therefore enhanced magnet coercivity without decreasing remanence and energy product.

1. Introduction

The realization of efficient electric vehicle motors or power generation systems for wind turbines necessitates the development of high-performance permanent magnets, which is associated with a number of challenges. Since their discovery in 1984 [1,2], high-coercivity sintered Nd-Fe-B magnets have found numerous practical and industrial applications, e.g., as components of actuators, motors, and generators [3]. However, the above applications require long-term magnet operation in high-temperature environments without any coercivity decrease, which is a non-trivial criterion. Generally, the coercivity of Nd-Fe-B magnets at room temperature can be enhanced by the partial replacement of Nd by Dy, Tb, or both; however, the high cost and scarcity of these rare earths preclude the widespread application of this method [4–9] and necessitate the development of more economically viable alternatives. One of such alternatives is the reduction of heavy rare earth element (e.g., Dy and Tb) usage and minimization of remanence and energy product loss via the utilization of the grain boundary diffusion process (GBDP, developed in 2000) [10,11].

Cao et al. fabricated sintered Nd–Fe–B magnets containing less than 1.44 wt% Tb by grain boundary diffusion of TbF_3, showing that they exhibit a maximum coercivity of ~28.12 kOe [12] and therefore demonstrating that the grain boundary diffusion of Dy or Tb compounds is expected to be an effective method for enhancing magnet coercivity [13–18]. However, most of the above studies were carried out using small-scale magnets because of the difficulty of diffusion process investigation in large-size industrial Nd-Fe-B magnets. Moreover, different heat treatment processes are expected to be required for optimized grain boundary diffusion in large-size industrial magnets [14,15]. Despite the importance of understanding the optimized heat treatment process and grain boundary diffusion mechanism in such large magnets, no systematic investigations have addressed this issue so far. Herein, we

* Corresponding author.
** Corresponding author.
E-mail addresses: jw.roh@knu.ac.kr (J.W. Roh), wooyoung@yonsei.ac.kr (W. Lee).
[1] S. Kim and D.-S. Ko contributed equally to this work.

https://doi.org/10.1016/j.jallcom.2018.11.412
0925-8388/

employ consecutive heat treatment–driven TbH diffusion to fabricate large-size Nd-Fe-B magnets exhibiting enhanced coercivity without any decrease of remanence (B_r) and energy product ($(BH)_{max}$). Furthermore, we systemically investigate the microstructure of Tb-diffused Nd-Fe-B magnets, revealing the relationship between Tb-diffused area and enhanced coercivity.

2. Experimental

A commercial 48M Nd-Fe-B sintered magnet (Ningbo Jinji Strong Magnetic Materials Co., Ltd.) with a size of 12 × 12 × 5 mm was used as a base magnet, and its surface was etched prior to the diffusion process to enable the efficient coating of diffusion source materials. A terbium hydride (TbH; Lumi M Co., Ltd.) powder – ethanol (1:1, w/w) slurry was aged for three days to remove hydrogen gas generated during slurry production, and the aged slurry was used as a Tb diffusion source. The sintered magnets were dip-coated into the above slurry, held at 900–960 °C for 6 h in vacuum for GBDP, and then subjected to two consecutive heat treatments (860–960 °C for 10 h and 440–520 °C for 2 h under Ar). After each heat treatment, the sintered magnets were quenched by quick injection of cold Ar gas.

For GBDP and heat treatment optimization, each process was carried out within different temperature ranges. Magnetic properties were measured using a BH hysteresis loop tracer (Permagraph C-300, Magnet-Physik), and microstructures were investigated using high-resolution X-ray diffraction (HR-XRD; SmartLab, Rigaku) and electron probe microanalysis (EPMA; JXA 8530F, JEOL).

3. Results and discussion

Fig. 1 shows the schematics of the Tb diffusion process during stepwise annealing process. The use of stepwise annealing allowed the diffusion of Tb through grain boundaries and further into the lattice with excess Tb, at the GBDP stage. The conditions of GBDP and first and second heat treatments were independently optimized, as demonstrated in Fig. 2(a), (b), and (c), respectively. In previous reports on the mechanism of diffusion in small-sized magnets (<25 mm^3), the dwelling time of high-temperature heat treatment was controlled to equal 1–7 h [17–24]. However, such short-term heat treatment is not efficient for the diffusion of atoms in large-volume samples, since the diffusion rate is mostly constant within a certain temperature range. In general, these relatively short heat treatments were not enough to induce the diffusion of Tb or Dy into the inside of our large-sized magnets (720 mm^3). In particular, when these magnets were annealed for 16 h at 940 °C, their coercivity was measured to be as low as 23.4 kOe, which suggested that prolonging the GBDP treatment time at constant temperature is not an effective way of magnetic property optimization. Therefore, the first heat treatment after the GBDP was performed at 900 °C.

Fig. 3 reveals that the coercivity of the base magnet increased by 62.7% (from 15.28 to 24.86 kOe) after the second heat treatment, whereas B_r and $(BH)_{max}$ concomitantly decreased by 1.66% (from 13.89 to 13.66 kG) and 1.43% (from 46.72 to 46.05 MGOe), respectively, as summarized in Table 1. Since antiferromagnetic coupling between Tb and Fe in sintered Nd-Fe-B magnets generally results in a decrease of B_r and $(BH)_{max}$ with increasing coercivity [5,15], the above result shows that consecutive heat treatment can efficiently enhance coercivity with a negligible decrease of B_r and $(BH)_{max}$. Fig. 4 and Fig. S1 show the XRD patterns of the (Tb-free) base magnet and magnets obtained after GBDP, first heat treatment, and second heat treatment. The enlarged XRD patterns in the region of $2\theta = 25–35°$ clearly show peaks of a rare-earth (RE)-rich phase (formed by the consecutive heat treatment) that partially replaced Nd atoms in $Nd_2Fe_{14}B$ via grain boundary diffusion of Tb atoms to afford a Nd-rich phase at the grain boundary.

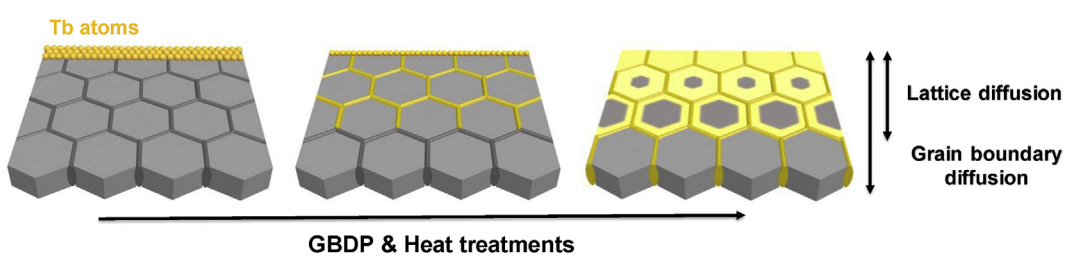

Fig. 1. Schematic illustration of Tb diffusion from the magnet surface during stepwise annealing.

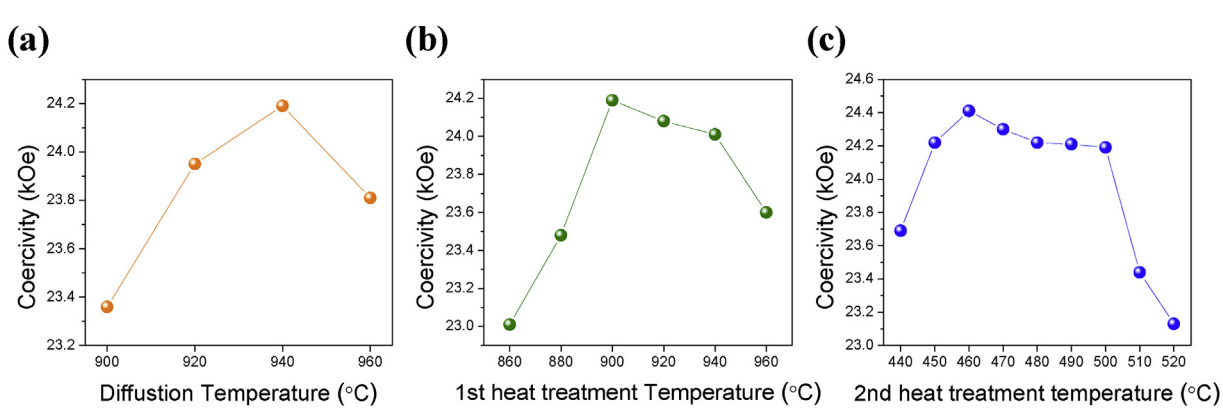

Fig. 2. Optimization of (a) grain boundary diffusion, (b) first heat treatment, and (c) second heat treatment conditions.

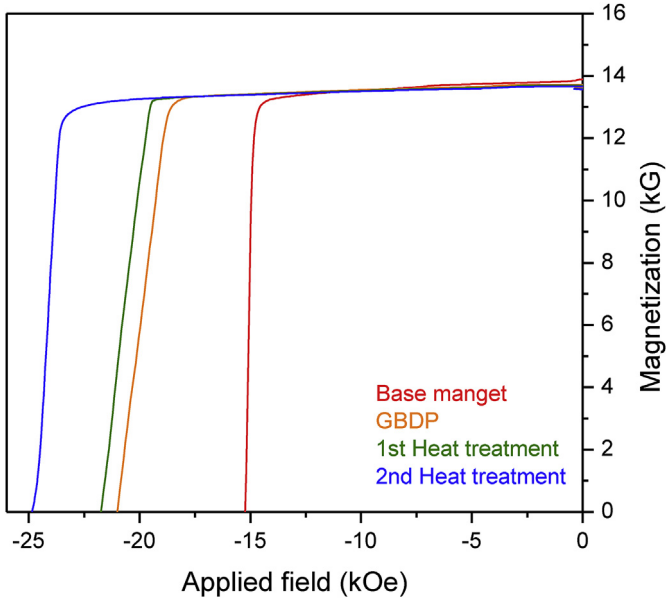

Fig. 3. Demagnetization curves of the base magnet and magnets obtained after GBDP, first heat treatment, and second heat treatment.

Table 1
Magnetic properties of the base magnet and magnets obtained after GBDP, first heat treatment, and second heat treatment.

Sample	H_{ci} (kOe)	B_r (kG)	$(BH)_{max}$ (MGOe)
Base magnet	15.28	13.89	46.72
GBDP	21.04	13.72	46.33
1st heat treatment	21.78	13.69	46.11
2nd heat treatment	24.86	13.66	46.05
Variance	+62.7%	−1.66%	−1.43%

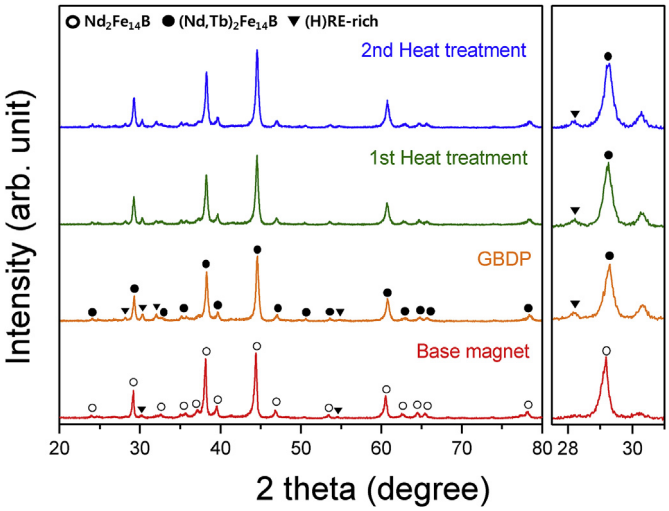

Fig. 4. XRD patterns of the base magnet and magnets obtained after GBDP, first heat treatment, and second heat treatment.

The microscale distribution of the RE-rich phase after each heat treatment was determined by EPMA. Fig. 5 shows EPMA mappings obtained along the depth direction from the surface of each magnet, demonstrating that Tb started to diffuse into the grain boundaries of the $Nd_2Fe_{14}B$ base magnet during the GBDP (Fig. 5(b)), reaching deeper under the surface during the first heat treatment (Fig. 5(c)). In contrast, the behavior observed during the second heat treatment was more complicated and featured two unique phenomena, namely the acceleration of Tb grain boundary diffusion and through-lattice Tb diffusion into grains, which resulted in the formation of two types of core-shell structures (Fig. 5(d)). Core-shell structures of the first type comprised Tb-rich $(Tb,Nd)_2Fe_{14}B$ grains as cores surrounded by shells with lower concentration of Tb. These Tb-rich grains were produced by the through-lattice diffusion of Tb, which allowed Tb to spread into the inside of the $Nd_2Fe_{14}B$ main phase by displacing Nd. The second structure type featured $(Tb,Nd)_2Fe_{14}B$ grains surrounded by shells with a higher Tb concentration. Notably, core-shell structures of the first type were observed at depths of up to 17 μm for the GBDP sample (Tb mapping images of Fig. 5(b)) and up to 88 μm for the sample obtained after the second heat treatment (Tb mapping images of Fig. 5(d)), which suggested that grain boundary diffusion proceeded through-lattice diffusion. In other words, the diffusion behavior of Tb changed from grain boundary diffusion to through-lattice diffusion, and the latter was the dominant process during the second heat treatment. The two-step diffusion of Tb was rationalized by the so-called Fisher model, which is commonly used to explain diffusion kinetics in polycrystalline materials [25,26]. In addition, after the second heat treatment, the microstructure of the central region of the magnet located vertically far from the surface was investigated using EPMA. As shown in Fig. S2, similar distributions of Nd and Tb were obtained for regions located at vertical distances of 1.25 and 2.50 mm from the surface, which suggested that the above metals sufficiently diffused into the whole magnet. Fig. 5(a) seems to suggest that Tb was uniformly distributed in the base magnet. However, the base magnet was a 48M magnet and did not contain Tb. Although we could not observe any Tb in EPMA spectra, the inevitable presence of noise during quantification through EPMA mapping could result in the false detection of Tb.

The phase changes of samples during processing were investigated by examining ternary diagrams constructed based on EPMA mapping images. The magnet subjected to the grain boundary diffusion process was regarded as a multiphase system, and the construction of ternary diagrams from EPMA maps allowed us to precisely obtain quantitative compositional information on individual phases for each heat treatment process [27]. Fig. 6 shows ternary diagrams obtained based on EPMA mapping images in Fig. 5. As shown in the Tb-Nd-Fe ternary diagram of Fig. 6(a), the areas of both Tb-rich $(Tb,Nd)_2Fe_{14}B$ grain and Nd (area 1) regions increased with increasing heat treatment time. As shown in the Tb-Nd-O ternary diagram of Fig. 6(b), the influx of Tb induced by heat treatment increased the Tb content of the entire region. In addition, Tb-replaced Nd diffused out of the grains, increasing the Nd contents of other regions such as the Nd-rich phase at grain boundaries (area 2). This result was in agreement with those of XRD analysis, confirming that the formation of the RE-rich phase was caused by the partial replacement of Nd atoms in $Nd_2Fe_{14}B$ with Tb atoms diffused from the surface and as well as by the formation of a Nd-rich phase at grain boundaries. To examine phase changes as functions of depth and heat treatment conditions, the distributions of Nd and Tb were examined by EPMA at depths of 30 and 80 μm below the surface (Fig. 7). The obtained results demonstrated that no significant differences were observed for depths of 30 and 80 μm after the first heat treatment (Fig. 7(a) and (b)), while the extent of Tb diffusion into the grain inside was significantly more pronounced for 30 μm than for 80 μm (Fig. 7(c) and (d)) after the second heat treatment. This observation revealed that during the second heat treatment, the lattice diffusion of Tb dominated over grain boundary diffusion.

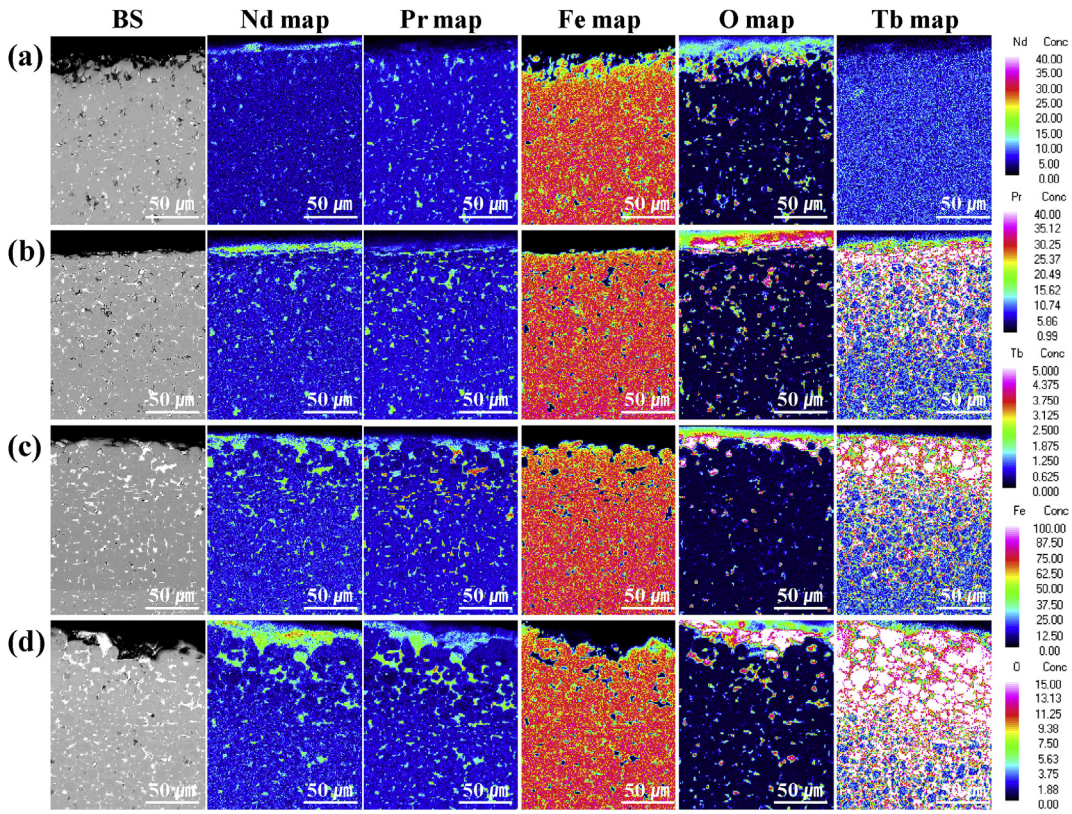

Fig. 5. EPMA profiles of (a) the base magnet and magnets obtained after (b) GBDP, (c) first heat treatment, and (d) second heat treatment.

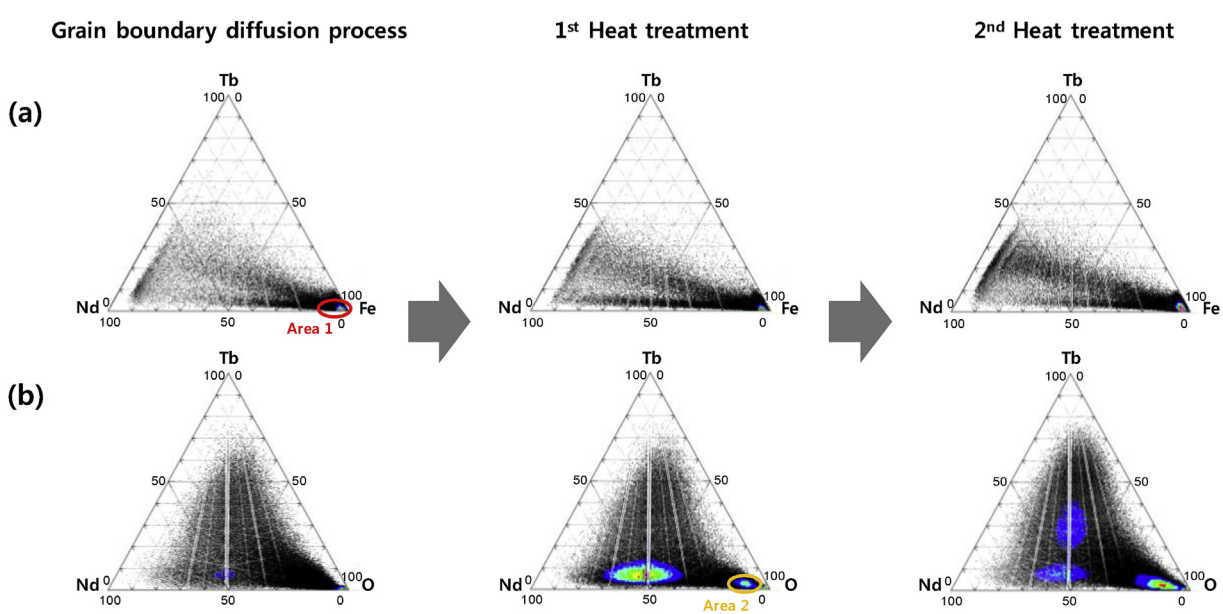

Fig. 6. Ternary diagrams constructed based on EPMA profiles from the images of Fig. 5.

The EPMA images of Figs. 5 and 7 were used to construct and analyze the Tb-Nd-O ternary diagram in Fig. 8. For a depth of 30 μm, region A in the Tb-Nd-O ternary diagram represents the area corresponding to Tb-rich $(Tb,Nd)_2Fe_{14}B$ grains obtained as a result of lattice diffusion and the grain boundary phase of core-shell structures with Tb-rich $(Tb,Nd)_2Fe_{14}B$ shells, whereas the grain phase of these core-shell structures appears in region B. Notably, the area representing Tb-rich $(Tb,Nd)_2Fe_{14}B$ grains increased after the second heat treatment because of lattice diffusion, which was in agreement with the results of EPMA imaging (Fig. 7(a) and (c)). For a depth of 80 μm, core-shell structures with Tb-rich $(Tb,Nd)_2Fe_{14}B$ shells are represented by regions C (grains) and D (grain

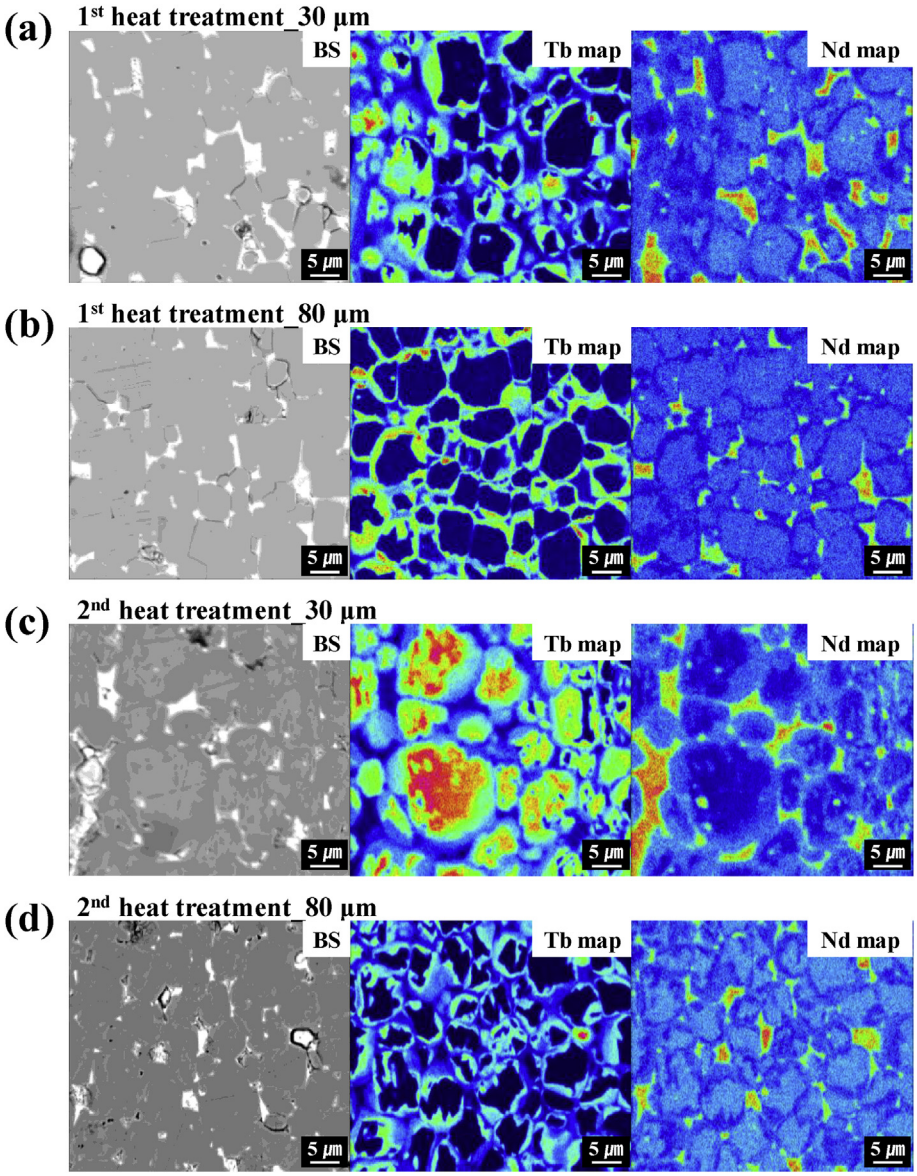

Fig. 7. EPMA profiles of magnets obtained after (a, b) the first heat treatment and (c, d) the second heat treatment at depths of (a, c) 30 μm and (b, d) 80 μm.

boundaries), with an increase of region D area observed after the second heat treatment. The further influx of Tb during the second heat treatment resulted in substitution of additional Nd and thus increased the amount of the Nd-rich phase at the triple junctions of grain boundaries (region E). The core-shell structure corresponding to regions C and D suppressed reverse domain nucleation at Nd-rich phase/main phase interfaces and is known to be the most efficient microstructure for improving coercivity while minimizing decreases of both B_r and $(BH)_{max}$ [20,24,28,29]. Kronmüller et al. [30] and Thompson et al. [31] reported that the crystal anisotropy of magnetic grains in the surface region, especially at corners and edges, is always lower than that of the grains inside, which leads to an obvious reduction of the magnetic reversal nucleation field and magnet coercivity. Therefore, even though the formation of Tb-rich $(Tb,Nd)_2Fe_{14}B$ grains (region A of Fig. 8(a) and (b)) may not be ideal from the viewpoint of economics in view of the rather high consumption of Tb, the formation of a lattice diffusion layer with certain minimum thickness and a higher magnetocrystalline anisotropy can provide enhanced protection against demagnetization at the magnet surface. In other words, the combination of GBDP and sequential heat treatment allows the formation of microstructures for improving coercivity while minimizing decreases of both B_r and $(BH)_{max}$.

4. Conclusions

The relationship between Tb-diffused area and coercivity enhancement was determined by probing the microstructure of Tb-diffused Nd-Fe-B magnets by EPMA and analyzing the obtained ternary diagrams. As a result, stepwise annealing was shown to generate core-shell structures via the combined effects of Tb lattice diffusion and grain boundary diffusion. For Nd-Fe-B sintered magnets of relatively large size, GBDP followed by a series of heat treatments including an additional first heat treatment at high temperature was concluded to be an effective method of enhancing coercivity without decreasing B_r and $(BH)_{max}$.

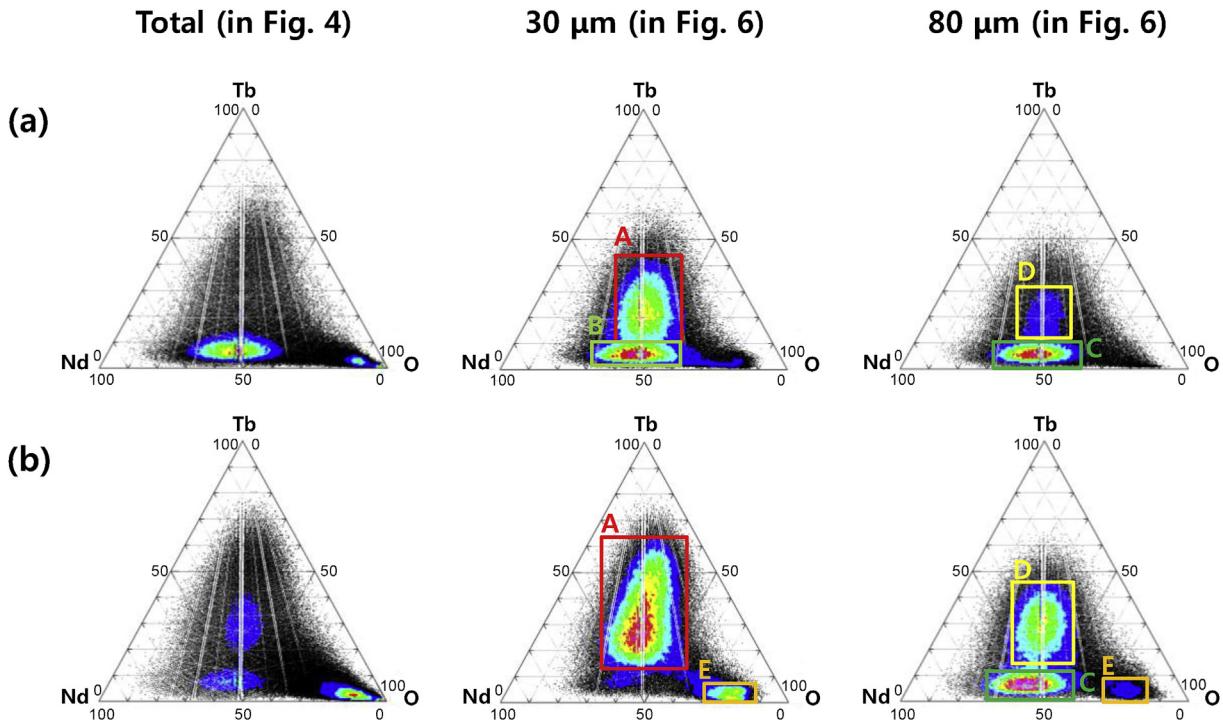

Fig. 8. Ternary diagrams obtained based on EPMA profiles in Figs. 5 and 7 for magnets after (a) the first and (b) the second heat treatment.

Acknowledgements

This work has supported by the National Research Foundation of Korea (NRF) grant funded by the Korean government (MSIT) (NRF-2018R1A2B6007169), and Priority Research Centers Program (2009-0093823).

Appendix A. Supplementary data

Supplementary data to this article can be found online at https://doi.org/10.1016/j.jallcom.2018.11.412.

References

[1] M. Sagawa, S. Fujimura, N. Togawa, H. Yamamoto, Y. Matsuura, New material for permanent magnets on a base of Nd and Fe, J. Appl. Phys. 55 (1984) 2083.
[2] J.J. Croat, J.F. Herbst, R.W. Lee, F.E. Pinkerton, Pr-Fe and Nd-Fe-based materials: a new class of high-performance permanent magnets, Appl. Phys. 55 (1984) 2078.
[3] O. Gutfleisch, M.A. Willard, E. Bruck, C.H. Chen, S.G. Sankar, J.P. Liu, Magnetic materials and devices for the 21st century: stronger, lighter, and more energy efficient, Adv. Mater. 23 (2011) 821–842.
[4] S. Hirosawa, Y. Matsuura, H. Yamamoto, S. Fujimura, M. Sagawa, H. Yamauchi, Magnetization and magnetic anisotropy of R2Fe14B measured on single crystals, J. Appl. Phys. 59 (1986) 873–879.
[5] J.F. Herbst, $R_2Fe_{14}B$ materials: intrinsic properties and technological aspects, Rev. Mod. Phys. 63 (1991) 819.
[6] O. Gutfleisch, Controlling the properties of high energy density permanent magnetic materials by different processing routes, J. Phys. D Appl. Phys. 33 (2000) R157–R172.
[7] D. Bauer, D. Diamond, J. Li, D. Sandalow, P. Telleen, B. Wanner, US Department of Energy Critical Materials Strategy, 2010.
[8] S. Sugimoto, Current status and recent topics of rare-earth permanent magnets, J. Phys. D Appl. Phys. 44 (2011).
[9] K. Hono, H. Sepehri-Amin, Strategy for high-coercivity Nd–Fe–B magnets, Scr. Mater. 67 (2012) 530.
[10] K.T. Park, K. Hiraga, M. Sagawa, Effect of metal-coating and consecutive heat treatment on coercivity of thin Nd-Fe-B sintered magnets, in: H. Kaneko, M. Homma, M. Okada (Eds.), Proc. 16th Int. Workshop Rare-earth Magnets and Their Applications, 2000, pp. 257–264.
[11] H. Nakamura, K. Hirota, M. shimao, T. Minowa, M. Honshima, Magnetic properties of extremely small Nd-Fe-B sintered magnets, IEEE Trans. Magn. 41 (2005) 3844.
[12] X.J. Cao, L. Chen, S. Guo, J.H. Di, G.F. Ding, R.J. Chen, A.R. Yan, K.Z. Chen, Improved thermal stability of TbF3-coated sintered Nd-Fe-B magnets by electrophoretic deposition, AIP Adv. 8 (2018), 056222.
[13] K.-H. Bae, T.-H. Kim, S.-R. Lee, S. Namkung, T.-S. Jang, Effects of DyHx and Dy2O3 powder addition on magnetic and microstructural properties of Nd-Fe-B sintered magnets, J. Appl. Phys. 112 (2012), 093912.
[14] X. Cao, L. Chen, S. Guo, R. Chen, G. Yan, A. Yan, Impact of TbF3 diffusion on coercivity and microstructure in sintered Nd–Fe–B magnets by electrophoretic deposition, Scr. Mater. 116 (2016) 40–43.
[15] K. Loewe, D. Benke, C. Kübel, T. Lienig, K.P. Skokov, O. Gutfleisch, Grain boundary diffusion of different rare earth elements in Nd-Fe-B sintered magnets by experiment and FEM simulation, Acta Mater. 124 (2017) 421–429.
[16] A.M. Gabay, M. Marinescu, W.F. Li, J.F. Liu, G.C. Hadjipanayis, Dysprosium-saving improvement of coercivity in Nd-Fe-B sintered magnets by Dy2S3 additions, J. Appl. Phys. 109 (2011), 083916.
[17] Wei-Qiang Liu, Cheng Chang, Ming Yue, Jing-Shan Yang, Dong-Tao Zhang, Jiu-Xing Zhang, Yan-Qin Liu, Coercivity, microstructure, and thermal stability of sintered Nd–Fe–B magnets by grain boundary diffusion with TbH3 nanoparticles, Rare Met. 36 (9) (2017) 718–722.
[18] Xiao Yang, Shuai Guo, Guangfei Ding, Xuejing Cao, Jiling Zeng, Jie Song, Don Lee, Aru Yan, Effect of diffusing TbF3 powder on magnetic properties and microstructure transformation of sintered Nd-Fe-Cu-B magnets, J. Magn. Magn. Mater. 443 (2017) 179–183.
[19] Hee-Ryoung Cha, Kwang-Won Jeon, Ji-Hun Yu, Hae-Woong Kwon, Yang-Do Kim, Jung-Goo Lee, Coercivity enhancement of hot-deformed Nd-Fe-B magnet by grain boundary diffusion process using the reaction of NdHx and Cu nanopowders, J. Alloys Compd. 693 (2017) 744–748.
[20] M. Komuro, Y. Satsu, H. Suzuki, Increase of coercivity and composition distribution in fluoride-diffused NdFeB sintered magnets treated by fluoride solutions, IEEE Trans. Magn. 46 (2010) 3831–3833.
[21] H. Sepehri-Amin, T. Ohkubo, S. Nagashima, M. Yano, T. Shoji, A. Kato, T. Schrefl, K. Hono, High-coercivity ultrafine-grained anisotropic Nd–Fe–B magnets processed by hot deformation and the Nd–Cu grain boundary diffusion process, Acta Mater. 61 (2013) 6622–6634.
[22] Song-E. Park, Tae-Hoon Kim, Seong-Rae Lee, Dong-Hwan Kim, Seok Nam-Kung, Tae-Suk Jang, Magnetic and microstructural characteristics of Nd-Fe-B sintered magnets doped with Dy2O3 and DyF3 powders, IEEE Trans. Magn. 47 (2011) 10.
[23] F. Xu, J. Wang, X. Dong, L. Zhang, J. Wu, Grain boundary microstructure in DyF3-diffusion processed Nd-Fe-B sintered magnets, J. Alloys Compd. 509 (2011) 7909–7914.
[24] T.H. Kim, S.R. Lee, H.J. Kim, M.W. Lee, T.S. Jang, Simultaneous application of Dy-X (X=F or H) powder doping and dip-coating processes to Nd-Fe-B sintered magnets, Acta Mater. 93 (2015) 95–104.

[25] J.C. FISHER, Calculation of diffusion penetration curves for surface and grain boundary diffusion, J. Appl. Phys. 22 (1951) 74–77.
[26] L.G. Harrison, Influence of dislocations on diffusion kinetics in solids with particular reference to alkali halides, Trans. Faraday Soc. 57 (1961) 1191–1199.
[27] D.R. Snoeyenbos, D.A. Wark, J.-C. Zhao, Constructing ternary phase diagrams directly from EPMA compositional maps, Microsc. Microanal. 14 (2008).
[28] K. Hirota, H. Nakamura, T. Minowa, M. Honshima, Coercivity enhancement by the grain boundary diffusion process to NdFeB sintered magnets, IEEE Trans. Magn. 42 (2006) 2909–2911.
[29] H. Sepehri-Amin, T. Ohkubo, K. Hono, The mechanism of coercivity enhancement by the grain boundary diffusion process of Nd-Fe-B sintered magnets, Acta Mater. 61 (2013) 1982–1990.
[30] H. Kronmüller, Theory of nucleation fields in inhomogeneous ferromagnets, Phys. Status Solidi B 144 (1987) 385.
[31] Margarita P. Thompson, Edwin Chang, Aldo Foto, Jorge G. Citron-Rivera, Daad Haddad, Richard Waldo, Frederick E. Pinkerton, Grain-Boundary-Diffused Magnets: the challenges in obtaining reliable and representative BH curves for electromagnetic motor design, IEEE Electrif. Mag. 5 (2017) 19–27.